Matrix-dependent size modifications of iron oxide nanoparticles (Ferumoxytol) spiked into rat blood cells and plasma: Characterisation with TEM, AF4-UV-MALS-ICP-MS/MS and spICP-MS

Kenneth Nwoko, Andrea Raab, Lesley Cheyne, Dana Dawson, Eva Krupp, Jörg Feldmann

PII: S1570-0232(19)30484-2
DOI: https://doi.org/10.1016/j.jchromb.2019.06.029
Reference: CHROMB 21702

To appear in: *Journal of Chromatography B*

Received date: 24 March 2019
Revised date: 29 May 2019
Accepted date: 23 June 2019

Please cite this article as: K. Nwoko, A. Raab, L. Cheyne, et al., Matrix-dependent size modifications of iron oxide nanoparticles (Ferumoxytol) spiked into rat blood cells and plasma: Characterisation with TEM, AF4-UV-MALS-ICP-MS/MS and spICP-MS, Journal of Chromatography B, https://doi.org/10.1016/j.jchromb.2019.06.029

Matrix-dependent size modifications of iron oxide nanoparticles (Ferumoxytol) spiked into rat blood cells and plasma: Characterisation with TEM, AF4-UV-MALS-ICP-MS/MS and spICP-MS.

Kenneth Nwoko[a], Andrea Raab[a], Lesley Cheyne[b], Dana Dawson[b], Eva Krupp[a], Jörg Feldmann[a]

a. Trace Element Speciation Laboratory (TESLA), Dept. of Chemistry, University of Aberdeen, AB24 3UE, United Kingdom.
b. School of Medicine and Dentistry, Foresterhill, University of Aberdeen, AB25 2DZ, United Kingdom.

Corresponding author: *kenneth.nwoko@abdn.ac.uk, knwoko@gmail.com*

ABSTRACT

Engineered nanoparticles such as iron oxide (Fe_3O_4) nanoparticles (IONPs) offer several benefits in nanomedicine, notably as contrast agents in magnetic resonance imaging (MRI). Ferumoxytol, a suspension of IONPs (with a manufacturer's reported particle diameter of 27 nm-30 nm) was characterized as a standard by spiking into rat blood plasma and cell fractions. Nanoparticle separation, and characterization was investigated with asymmetric flow field-flow fractionation (AF4) coupled online to ultraviolet-visible spectroscopy (UV-VIS), multi-angle light scattering (MALS) and inductively coupled plasma mass spectrometry (ICP-MS) detectors; also with single particle inductively coupled plasma mass spectrometry (spICP-MS) and transmission electron microscopy (TEM). MALS signal of pristine Ferumoxytol indicated radii of gyration (R_g) between 15-28 nm for the Fe-containing fraction and 30-75 nm for the non-Fe fraction. IONPs spiked into blood plasma indicated a polydisperse distribution between 40 nm - 120 nm suggesting matrix-induced size alterations. Spiking of the IONPs into cells shows a shift in ICP-MS Fe signal to 15 min, however the MALS signal was undetected within the Fe containing fraction of the IONPs suggesting NP loss due to membrane-particle attraction. spICP-MS analysis of IONPs spiked in rat plasma suggested the release of Fe-containing colloids into plasma causing an increase in diameter of IONPs to 52± 0.8 nm; whereas no major variation in particle size and distribution of the IONPs spiked in cell fractions was observed (33.2 ± 2.0 nm) suggesting non-alteration of the NP Fe core. A complementary application of microscopic, light scattering, and mass spectrometry for the characterisation of NPs in challenging biological matrices like blood has been demonstrated.

Keywords: Ferumoxytol, nanoparticles, blood, plasma, cells

1. Introduction

Engineered nanoparticles are particles in the size range of 1-100 nm that are designed with specific intended properties and purposes. They have become increasingly useful in everyday life with applications across diverse sectors in products such as drugs, cosmetics, photovoltaic cells, surface coatings etc. In healthcare, engineered metallic nanoparticles (EMNPs) are now increasingly important in 'nanomedicine' for therapeutic as well as diagnostic purposes (nanotheranostics) [1,2] . The need to effectively and accurately deliver therapeutic load to target tissues across cell membranes is challenging to meet using conventional drugs, necessitating the development and use of biocompatible nano-sized particles as an alternative approach [3]. The unique properties of EMNPs such as high surface area/volume ratio, high reactivity, optical properties [4], and biocompatibility make them ideal candidates for such applications. Superparamagnetic iron oxide nanoparticles (SPIONs)[5-8] have been well studied for their use as diagnostic contrast agents for magnetic resonance imaging of diseased cardiovascular tissue[9], and are preferred over gadolinium-based contrast agents especially in certain conditions such as in patients with chronic kidney disease (CKD)[10,11], where better tolerances have been reported[12]. In addition, iron supplements are regularly administered intravenously for severe Fe deficiency anaemia especially in cases where oral iron supplementation is inadequate [13]. However, despite the obvious advantages of iron oxide nanoparticles (IONPs), concerns abound regarding their safety and possible toxicity arising from their intravenous administration with potential occurrences of toxic reactions[14,15] .For instance, supplementation of iron in patients with underlying dysfunctional Fe metabolism such as in thalassemia[16], increases the risk of cell necrosis due to the interplay between Fe and reactive oxygen species (ROS)[17]; with evidence suggesting toxicity due to Fe release following biodegradation of the Fe core in SPIONs[18], as well as reported cases of hypersensitivity by the Food and Drug Administration (FDA)[19] .

To better explain the interaction of intravenously injected IONPs within the circulatory system, there is a need to investigate NP size changes that may occur *in vivo*, particularly within the period (24 h) reported for normal systemic clearance. Phagocytosis of IONPs from macrophages resident in the spleen and bone marrow as well as liver cells have been reported to be the operative mechanism responsible for the rapid clearance of IONPs from reticulo-endothelial system (RES) circulation [20]. It is therefore an imperative to understand the fate

of the injected IONPs; whether they undergo rapid transformation or slow dissolution in blood. From an analytical perspective, there is a need to study *in vitro* the influence and extent of sample matrix effect on a characterized 'standard' IONPs when it is spiked into blood. Dynamic light scattering (DLS) and electron microscopy have been used to characterize IONPs marketed as Ferumoxytol, a commercial IONP suspension [21]; with variable particle sizes reported for the core Fe and surrounding polysorbitol carboxymethylether (PSC) coating [22].

However, apart from generating images, these imaging and counting techniques do not provide enough reliable information with respect to changes in the size and form of the IONP during transport and interaction with matrix components in blood. In addition, conventional NP techniques such as TEM may in some cases be impeded by complex preparative techniques and sample matrix effects such as evaporation. More importantly, the high abundance of Fe in biological systems necessitates a need to employ a combination of techniques that combine separation, size characterization, as well as element specific detection capability.

As previously acknowledged, no single technique can be applied to sufficiently identify, characterize and quantify NPs in a sample or scenario, rather a combination of techniques is required [23]. Asymmetric flow field-flow fractionation (AF4) is a gentle separation technique for the fractionation of NPs transported in a liquid carrier medium in a thin channel under the action of a perpendicular cross flow based on their diffusion coefficients, with a semi-permeable membrane acting as a an accumulation wall for the retention of nanoparticles[24,25]. The absence of a solid stationary phase enhances separation and reduces potential losses from analyte-column interactions. The AF4 fractionation system is equipped with a multi-angle light scattering (MALS) detector which has been applied for the accurate separation, particle size and molar mass characterization of polymers in drug delivery systems [26]. Multi-angle light scattering (MALS) detector generates a unique measurand for light scattering at various angles by individual particles of a macromolecule in solution known as the radius of gyration (R_g); defined as the root mean square distance of the object's mass from either its centre of mass or a given axis[27]. Coupling of AF4-UV-MALS with online an element-specific detector such as inductively coupled plasma mass spectrometry (ICP-MS) is robust and has been extensively applied to provide highly needed elemental identification of fractionated NPs as a complement to particle size in a variety of sample matrices [28-30]. Conventional mode ICP-MS enables the quantification of the total elemental

concentration of EMNPs in various sample matrices, provided that the artefacts, natural/background levels can be sufficiently differentiated from the target EMNPs. Use of radiolabelled or stable isotopes can overcome this challenge and enables the traceability of such labelled NPs in biological cells. However, some inherent shortcomings of this approach are the potential for radioactive contamination, need for special detectors and inability to conduct long-term studies when handling samples with short-half-life [31]. Another viable alternative is single particle ICP-MS (spICP-MS); which measures metallic NPs above high levels of natural/background dissolved analyte, enabling the detection of single particle signals as 'pulses' at very fast dwell times and ultra-low sample concentrations. In addition, with the destruction of the organic coating of the IONP in the ICP-MS plasma, the particle diameter of the ionized Fe-NP can be obtained without matrix interference [32,33]. In this study, AF4 was coupled with online UV-VIS, multi angle light scattering (MALS), and ICP-MS detectors to characterise an IONP, as well to investigate potential size changes due to sample matrix effect. In addition, spICP-MS was applied to investigate potential size changes to the metallic (Fe) core of the NP due to matrix effects. The objective of the study was the detection and sizing of the IONP in its unaltered form with minimal sample preparation. The IONPs will be spiked into rat blood plasma and cellular fractions with 24 h incubation and NP size characterisation performed using AF4-UV-MALS-ICP-MS/MS, TEM and spICP-MS.

2. Material and methods

2.1 Experimental

2.1.1 Reagents and standards. All reagents used were of analytical grade or better, except where otherwise stated. A 30 mg mL^{-1} suspension of an engineered IONP (as Ferumoxytol®) was supplied by the Cardiovascular Imaging Research Group, Institute of Medical Sciences, University of Aberdeen. De-ionised ultrapure water (18.2 MΩ cm) from a Smart 2 Pure Millipore water system (Thermo Scientific, Sweden) was used for preparation of the mobile phases and blank solutions. The mobile phase for AF4 was 0.2% *v/v* Novachem surfactant (Postnova Analytics) in ultrapure water. The Novachem surfactant is a mixture of anionic and non-ionic surfactants with a stated composition [34]. The mobile phase was subsequently filtered under vacuum through a 0.22 μm cellulose acetate filter prior to use. The nebulization efficiency was determined by measuring a commercial AuNP standard suspension (Nanocomposix, USA) with a certified median particle diameter of 56 ± 0.5 nm (TEM) and

50 mg kg^{-1} AuNP concentration. It was diluted 10^{-6} times with ultrapure water to yield a final working concentration of 50 *n*g kg^{-1}. Dissolved Fe elemental standards (Accustandard, New Haven, USA) with a concentration of 1 μg kg^{-1} were prepared in ultrapure water from the stock solution of 10 mg L^{-1} and used to measure elemental response factors.

2.1.2 Rat blood samples. Blood samples of adult rats were obtained from the Institute of Medical Sciences, University of Aberdeen and separated into plasma and cellular fractions by centrifugation. The cellular fractions were freeze dried for 12 hours (Heto Powerdry LL3000, Thermo Electron), and 50 mg fraction was dissolved in 10 mL of deionised water in acid washed sample tubes. Micro-sized particles were removed by filtering through a 0.45 µm syringe filter, and the filtrates were diluted with water.

2.1.3 Spiking of samples with Ferumoxytol standard. A working suspension of the IONP as a standard was prepared by dilution of 30 mg mL^{-1} of Ferumoxytol to a final concentration of 0.150 mg mL^{-1}. Working solutions of the samples were prepared by spiking equivalent volume of diluted Ferumoxytol suspension respectively into 1 mL aliquots of plasma and cellular fractions and incubated at 37°C for 24 hours.

2.1.4 Transmission electron microscopy (TEM). Samples were centrifuged for about 1 min, and 5 µL of the suspension fixed onto circular, Formvar-coated copper films (200 mesh size) with a diameter of 3.05 mm. The TEM films were left to air-dry at ambient room temperature for 10 mins prior to analysis.

2.1.5 Sample dilution (spICP-MS). To reduce the influence of soluble iron from haemoglobin which is naturally abundant in blood cells, micro-filtrates of the blood cell fraction were further centrifuged for 5 mins at 13,500 rpm and the supernatant was spiked with Ferumoxytol prior to dilution for spICP-MS. Ferumoxytol, plasma and filtered rat blood lysate samples were subsequently diluted to relevant concentrations with ultrapure deionised water.

2.2 Instrumental analysis

2.2.1 TEM. TEM images were acquired with a JEOL-1400 plus electron microscope, at an accelerating voltage of 80 kV, using an AMT UltraVUE camera. After image acquisition, they were filtered, and individual points counted as NPs using an open source image processing software (ImageJ); assuming a spherical morphology for the NPs. Particle

diameters were calculated from areas of individual spheres and the data subsequently exported to Microsoft Excel to plot size frequency histograms.

2.2.2 Coupling of AF4-UV-MALS to ICP-MS/MS. AF4 experiments were performed on an AF2000 MT system (Postnova Analytics, Landsberg, Germany). The separation system consisted of a solvent degasser, solvent organiser, two isocratic solvent pumps, a pair of Kloehn pumps for generation of the crossflow, an auto-sampler (PN 5300), and a separation channel. The separation channel was enclosed inside a thermostat consisting of a trapezoid cartridge, a ceramic frit and a spacer of 350 µm nominal height. Temperatures of 4°C and 25°C were maintained for the auto-sampler and oven respectively. The fractionation system was coupled to a UV-Vis detector, a 21 angle multi-angle light scattering (MALS) detector and an online interface for connection to ICP-MS; all signals were monitored simultaneously. The MALS detector consisted of 21 light scattering cells at angles between 7^{o} to 164^{o}, with a laser light intensity of 50 mW and wavelength of 532 nm. Light scattering detectors were normalized by injecting a suspension of a mixture of 60 nm, 125 nm, and 350 nm latex beads. Light scattering data was recorded across all 21 angles but only the 90° signal was reported, except where stated otherwise, with UV-VIS absorbance monitored at 280 nm wavelength. A sample volume of 20 µL was used throughout the experiment, except where otherwise stated. Adequate membrane conditioning and reproducibility was achieved with a minimum of triplicate injections per sample. Electronic signals generated from UV-VIS and MALS detectors were processed with the AF2000 software. Detailed AF4 elution conditions are shown in Table S1. ICP-MS/MS analysis was performed on an Agilent 8800 QQQ ICP-MS, fitted with a Micromist nebulizer and a double pass spray chamber. The ICP-MS/MS analysis parameters are outlined in Table S2.

2.2.3 spICP-MS analysis. Single particle ICP-MS analysis was performed on an Agilent 7900 ICP-MS equipped with a Micromist nebulizer and a double pass spray chamber. Nanoparticle signals were acquired at a dwell time of 100 μs. spICP-MS operating conditions are described in detail in Table S3. Instrumental parameters (lens position, torch position) were optimised daily to achieve maximum sensitivity with an aqueous tune solution of 10 $\mu g\ L^{-1}$ Li, Co, Y, Ce, Tl. Nanoparticle diameters for all the samples were reported as an average diameter of six replicates. Data analysis was performed using the Agilent MassHunter 4.4 software (Agilent Technologies, USA).

3. Results and discussion

3.1 TEM: TEM is a conventional technique for the characterisation of NPs in biological specimens and has also been applied for the characterisation of IONPs [35]. However, a major constraint when analysing NP suspensions from a biological matrix using TEM are occasional low resolution images which are caused by the introduction of artefacts during the drying stage in the preparation of the TEM grid. Figure 1a indicates the presence of a cluster of spherical and random shaped structures in the pristine IONP which suggest the detection of IONPs. From the size frequency histogram, (Figure S1), the equivalent circular diameters of the pristine IONP ranged from 10-40 nm, with an average particle diameter of 21± 0.5 nm.

Figure 1. TEM images of pristine IONP (top left), IONPs spiked into rat blood plasma (top right) and IONPs spiked into rat blood cell (bottom).

However, in the study by Wu *et al*. [22], IONPs as Ferumoxytol have been studied by both cryo-TEM and room temperature TEM showing diameters of between 5 to 9 nm prepared and measured with room temperature TEM; and an average hydrodynamic of diameter 25 nm obtained with DLS. Remarkably, the study showed that Ferumoxytol consisted of a structure of iron core clusters, which are composed of several iron-carbohydrate particles. The cluster structures suggest that the PSC coating surrounding Ferumoxytol iron cores might be shared among different iron cores. The increased particle diameters of IONPs from Ferumoxytol measured in this study therefore appear to be related to this cluster structure, as well as possible introduction of artefacts during room temperature sample preparation. In the IONPs spiked into blood plasma (Figure 1b), there appears to be an increased number of particles, with the dominance of irregularly shaped structures. However, size frequency histograms

(Figure S1) of the IONPs spiked into blood plasma showed a size population with equivalent circular diameter ranging from 15 nm to 50 nm (average diameter=18.0 ±5.2 nm). A hypothesis for this observation is that the iron cluster structure facilitated by the carbohydrate coating has been altered and the IONPs have disintegrated into smaller sized particles. The TEM images also indicate a change from spherical to rod-like morphology for the particles, which are now more dispersed within the matrix.

The TEM image from the IONPs spiked into blood cell sample (Figure 1c) showed a number of random shaped structures which appeared significantly larger than those seen in pristine IONP. The size frequency histogram of the spiked rat blood cell also resulted in a polydisperse size distribution with an average particle equivalent circular diameter of 111± 14 nm (Figure S1). The IONPs are suggested to form agglomerates which may be induced by magnetic attraction forces as shown in a similar study of superparamagnetic magnetite NPs spiked into calf serum [36]. Alternatively, it can also be suggested that the iron-carbohydrate cluster structure contributes to formation of aggregates and the increase in the sizes, when compared with the TEM image of a blood cell devoid of IONPs which shows only amorphous structures (Figure 2).

Figure 2. TEM image of a blood cell extract devoid of IONPs.

Despite the lower image resolution characteristic of room temperature TEM compared with images obtained from advanced techniques such as cryo-TEM, the images provides some evidence that when the pristine IONPs were spiked into blood plasma their morphology was altered to show more rod-like morphology and the IONPs became more dispersed. The TEM images of IONPs spiked into cells also suggest larger sized irregular shaped structures; but

from both specimens it is challenging to confirm if these are aggregated NPs because of the limitation of a low resolution of TEM. The polymeric coating of the IONPs in this case PSC are surface active [37] and may cause bias during TEM analysis. Thus, to achieve more accurate characterisation using conventional TEM in a biological matrix, the application of advanced TEM techniques will provide an enhanced image resolution and reduce the possibility of artefact formation during sample preparation.

3.2 AF4-UV-MALS coupling to ICP-MS/MS: In brief, asymmetric flow field-flow fractionation (AF4) is a technique for the sequential separation of nanoparticles and colloids in a thin channel under the action of a perpendicular crossflow. NPs are separated sequentially, eluting in order of increasing particle size and characterized as an ensemble by the UV and MALS detectors, while ICP-MS enables element specific detection. From FFF theory, retention time t_r is directly proportional to particle hydrodynamic diameter d_H as shown in the equation below [38]:

$$d_H = \left(\frac{2kTA}{\pi\eta V_c w t^o}\right).t_r$$

Where, $d_{\mathrm{H}=}$ Particle hydrodynamic diameter, $k =$ Boltzmann constant, $T =$ Absolute temperature, A=Area of the accumulation wall, V_c= Cross flow rate, $\eta =$ Viscosity of mobile phase, $w =$ Channel thickness, $t^o =$ void time, $t_r =$ Retention time.

Though it was not applied in this study, the use of buffer solutions such as phosphate buffer saline (PBS) at physiological pH as AF4 mobile phases may appear suitable for biological samples but there are peculiar associated analytical problems such as salt precipitation which cause blockages in the AF4 system. The use of buffers as mobile phase in AF4 have been associated with loss of NP surface charge and aggregation [39,40]. As such, use of surfactant based mobile phases shows faster elution, better separation, peak reproducibility and higher

recovery rates because they shield the NP from unwanted interactions with the membrane which is considered a bigger advantage than a potential disadvantage of particle size over-estimation [41]. The same surfactant used in this study has been applied for previous AF4 separation and characterisation studies of SPIONs [42,43].

The recovery rates (Table S3) and elution times of the pristine IONPS recorded with various crossflow programmes (1 mL min^{-1}, 2 mL min^{-1}, 3 mL min^{-1}) were compared (UV-MALS and ICP-MS signals) to ascertain the optimal crosslow programme for the separation of IONPs (Figure S2 and Figure S3). Gigault *et al*. [44] consider an elution programme with a recovery rate of 70% to be adequate in an AF4 separation. From assumptions of FFF theory, membrane-particle interactions are absent during an ideal NP crossflow fractionation. In reality however, particles may be attracted and become irreversibly attached to the membrane leading to sub-optimal recovery rates. The 1 mL min^{-1} elution programme showed the highest NP recovery rate (79%) and elution time (10 min) for the pristine IONPs and therefore was applied for the characterisation of the pristine IONPs as a standard (Figure 3). Elution time differences of the IONPs for the 2 mL min^{-1} and the 3 mL min^{-1} crossflows were subtle; however 2 mL min^{-1} (R=74%) showed a higher recovery than 3 mL min^{-1} (R=69.5%). Also, all the three crossflow programmes showed an intense MALS peak at t_0, suggesting some pre-elution of unfractionated particles. A possible cause for suboptimal recoveries of the injected IONPs was speculated to be due to membrane-particle interactions, which was investigated by measuring a blank as a wash-out step without crossflow after each injection of pristine IONPs using the different crossflow programmes (Figure S4). From MALS and ICP-MS signals, sample carry-over was detected for the crossflow programmes, the mass of Fe released was inversely proportional to the crossflow rate (Figure S2 -S4). However, the 2 ml crossflow recorded the least intense UV-VIS peak at t_0 (Figure S2a) and showed better separation of the IONP into two distinct MALS fractions. Thus, with its higher field strength,

the 3 mL min^{-1} programme might be unsuitable to be used as an optimal crossflow rate in view of a higher possibility of membrane adhesion. Consequently, the 2 mL min^{-1} crossflow programme was considered as an optimal crossflow as a way to achieve a compromise between recovery rate and a gentle fractionation of the species. It was also considered it to be an optimal crossflow rate for the fractionation of any species that may be formed after the spiking of IONPs into blood fractions as it showed two well-resolved MALS peaks which may correspond to the iron and non-iron fraction respectively. A random coil fit model was also applied for R_g computation because it showed an excellent fit across the 21 light scattering angles of the MALS detector.

Figure 3. AF4-UV-MALS-ICP-MS/MS fractograms showing the detection of Fe-containing particle in a pristine IONP sample using a 1 mL min^{-1} crossflow elution programme. The radius of gyration (b) of the IONPS were computed from MALS signals based on a random coil fit model.

Figure 3 illustrates the detection of UV-VIS and ICP-MS signals at 10 min, confirming that the fraction was an Fe-containing particle. However, MALS signal showed the elution of two peaks which are not clearly resolved between 10-20 min and 20-30 min respectively. The broken line (Figure 3b) indicates the separation between the two fractions; the peak eluting between 20 – 30 min was a non-iron containing peak and may be suggested to be part of the PSC coat. The radius of gyration obtained from integration of the light scattering signals using a random coil fit model showed a size range of between 15 nm and 28 nm (R_g=23 nm)

for the first fraction while the 2nd fraction showed a radius of gyration distribution between 30 nm to 75 nm (R_g =47.5 nm). Thünemann *et al*. [42] reported the characterisation of another commercial brand of SPIONs (Resovist) with AF4 coupled with small angle x-ray scattering (SAXS). 99% Particles displayed a bimodal size distribution, with 99 % particles in a radius of 4 – 13 nm, while 1% of the particles extended up to 21 nm. A bimodal distribution was clearly observed in this study using the 2 mL^{-1} and 3 mL^{-1} crossflow programmes. The MALS signal at t_0 showed a higher intensity than UV-VIS which is speculated to indicate the elution of unfractionated particles at the start of the run. However, in both studies two different commercial brands of SPIONs were studied (Ferumoxytol vs. Resovist) which were composed of particle cores of magnetite (Fe_3O_4) and maghemite (γ-Fe_2O_3) respectively. Therefore, in view of possible subtle differences in NP chemistry, it is challenging to draw a valid conclusion in terms of similarity of their particle size distributions.

Figure 4. AF4-UV-MALS-ICP-MS/MS fractograms depicting the detection of IONPs spiked into rat blood plasma (a) and a non-spiked plasma sample (b). The radii of gyration distributions of NPs detected for IONPs spiked into plasma (c) and a non-spiked plasma sample (d) were computed from integration of MALS electronic signals based on a random coil fit model.

From Figure 4a, UV-VIS, MALS and ICP-MS signals were detected in the plasma sample spiked with Ferumoxytol at 6 min and at 10 min, suggesting that the IONP may have assumed a polydisperse form in the plasma sample matrix. A MALS peak at t_0 (4.8 min) suggests the detection of a small number of unfractionated particles which have also been earlier observed in the fractionation of the pristine IONPs (Figure 3). The radius of gyration distribution between 6-10 min (Figure 4c) ranges between 40 nm-60 nm (average R_g =

49 nm) which was likely composed of the original IONPs (detected at t_r= 10 min). It can also be suggested that the IONPs have undergone some destabilisation resulting to a fragmentation of the IONPs. From 10 min to 30 min the MALS signal shows a broad peak, with an R_g of between 40 nm to 120 nm. The evidence from the MALS size distribution therefore suggests that the IONPs may have agglomerated after interaction with plasma proteins. Previous studies have reported that the abundant number of proteins in blood plasma bind to the surface of IONPs of different sizes [45]. The random coil fit model shows a good data fit which suggests that a non-spherical morphology for the IONPs when spiked into plasma thereby partially supporting the evidence provided with TEM images. However, the R_g values from MALS signals are far higher than the average diameters calculated from TEM images, which can be explained by the fact that TEM particle size determination from image treatment using Image J assumes a spherical morphology which yields an 'equivalent circular diameter', contrary to the actual visualisation of rod-like particles. Also, from a previous study [46] this discrepancy between TEM diameter and MALS R_g has been attributed to the influence of the encapsulating polymer coating (in this case polysorbitol carboxymethylether, PSC). However the low resolution of TEM in this study does not provide enough evidence for this assertion.

In the non-spiked plasma sample (Figure 4d), intense UV-VIS, MALS and ICP-MS peaks were recorded at 6 min. ICP-MS signal suggests this to be small sized iron containing colloids in plasma (28-35 nm) , or erythrocytes which have been released from lysis during centrifugation of whole blood. In addition, the MALS signal between 20-30 min (Figure 4c) is elevated in the spiked sample compared to the non-spiked plasma sample (Figure 4d) showing a size distribution of 50 nm – 120 nm, suggesting the detection of some non-iron containing background colloids or artefacts.

Figure 5. AF4-UV-MALS-ICP-MS fractograms showing the detection of IONPs into blood cells spiked into Ferumoxytol (a), and of non-spiked blood cells (b). Radii of distribution of IONPs spiked into blood cells (c) and of non-spiked blood cells which were computed from integration of MALS signals based on a random coil fit model.

In the blood cells with spiked with Ferumoxytol (Figure 5a), ICP-MS and UV-VIS peaks were detected between 10 and 20 min with a peak maximum at 15 min, but a MALS signal was not detected. The UV-VIS peak was also of reduced intensity compared with the pristine IONPs. Compared to the pristine IONPS (t_r= 10 min), a slight shift in ICP-MS retention time (t_r= 15 min) suggested that the IONPS may have interacted with the membrane in a different manner causing particle adhesion on the membrane. A low intensity MALS signal is an indication that the particles are below the detection limit of the MALS signal. Alternatively, this may also suggest that the core-shell structure of the IONP has become destabilised. In this manner, the carbohydrate coating appears to have disintegrated in the cellular matrix such that the exposed IONP core adheres to the membrane. Possible mechanism of adhesion could be related to electrostatic (attractive) forces, or magnetic effect. At t_0 (5 min), intense UV-VIS, MALS and ICP-MS peaks were observed in the spiked blood cell sample which may be unfractionated particles or background iron-containing material.

In the non-spiked cell sample, intense UV-VIS, MALS and ICP-MS peaks were also observed at t_0, and are suggested to be cellular iron containing biomolecules in the blood cell matrix. However, MALS signal showed a broad peak dispersion between 20 min and 40 min with an R_g in the range 40 nm to 160 nm in both the non-spiked blood cell and spiked samples (Figures 5c and 5d). This can be attributed to the presence of background cellular

material which remains unchanged with the injection of the IONPs. It can be suggested that the surface charge of the IONPs is shielded by the surfactant hydration layer which causes repulsion between the IONP and the endogenous biomolecules in the cellular matrix.

3.3 Single particle ICP-MS. In spICP-MS analysis, samples must be sufficiently diluted and measured in fast time resolved analyis (TRA) mode using a short dwell time. When a single NP enters the plasma, a packet of ions is generated which creates a pulse signal on reaching the detector. The detector pulse is correlated to the total mass per particle, and subsequently correlated to the particle size [47]. The nebulisation efficiency [48,49], a key parameter for the determination of particle size distribution was obtained from analysis of a 50 *n*g kg^{-1} suspension of a AuNP standard (Figure S4).

Figure 6. Time scan of Fe signal for 150 ng kg-1 IONPs (Ferumoxytol), detected with sp-ICP-MS using a 0.1 ms dwell time (a); particle size distribution of pristine IONPs (b) obtained using the MassHunter software showing a indicating a median particle diameter of 28±3.2 nm.

Processing of signals with the MassHunter software resulted to a median particle diameter of 28±3.2 nm, which represented the diameter of the metallic core of the IONP with a narrow distribution suggesting monodispersity (Figure 6). This value is mathematically equivalent to a radius of 14± 1.6 nm, which is less than the average gyration radius of 23 nm determined with MALS detector for the Fe-containing fraction of Ferumoxytol; which difference can be attributed to the PSC carbohydrate coating . The frequency size distribution (Figure 5b) indicated that the particles were < 50 nm which appears valid considering the 10 nm limit of size detection (LOSD), or minimum diameter (D_{min}) using the atomic weight of Fe (56 g mol^{-}

[1]). Despite such impressive LOSD, the 10 – 15 nm particles cannot be visualised on the histogram and are assumed to be detected alongside background noise signals. The LOSD indicates an improvement in the D_{min} of 55 nm for iron (as ^{56}Fe), and 102 nm (as Fe_3O_4) using a dwell time of 10 milliseconds reported in a study by Lee *et al*. [50]. Two factors were responsible for lowering of the LOSD; use of collision cell technology (CCT) which reduces background noise (and instrument sensitivity), and a shorter dwell time which increases particle counting frequency and reduces the detector's chance of omitting a particle. In this study, the collision cell was flushed with 3.5 mL min^{-1} of H_2 gas to completely remove potential interference from $^{40}Ar^{16}O$ species in ICP-MS argon plasma. Furthermore, a nebulizer gas flow rate of 0.79 L min^{-1} and a torch with 1.0 mm internal diameter were also used to minimise background noise. However, these measures were liable to cause a drop in instrumental sensitivity; but in the case of iron, a drop in sensitivity may be less impactful considering the high isotopic abundance of ^{56}Fe (92%), and the overall high concentration of iron in the sample matrix. The use of a 0.1 millisecond dwell time in this study also causes a reduction of the LOSD and compensates for the drop in instrument sensitivity as shown in the timescan of a blank ultrapure deionised water sample (Figure 7) .

Figure 7. Timescan of a blank sample (milli Q) measured at the start of the experiment to ascertain complete removal of interfering polyatomic species.

The discrepancy between the particle radii of the pristine IONPs from spICP-MS (14 nm) and MALS detector (23 nm) may be attributed to the presence of a hydration/corona layer around a particle in solution; however the R_g values may be over-estimated with the use of a surfactant based AF4 mobile phase. Considering that the pristine IONPs were engineered NPs and therefore monodisperse, a comparable particle diameter should be expected from spICP-MS and TEM analysis according to a previous study of engineered gold NPs by Pace *et al*. [33] which reported diameters of 37 nm and 42 nm using spICP-MS and TEM respectively. Therefore, this study suggested a considerable discrepancy between the spICP-

MS median diameter (28 nm) and TEM average diameter (21 nm). Interestingly, spICP-MS diameter of the pristine IONPs correlated with the manufacturer's nominal diameter of 30 nm which can be attributed to the high sensitivity of the spICP-MS technique such that the fast NP acquisition time (dwell times) of 0.1 ms ensured an improved counting and sizing of the IONPs.

Figure 8. Time scan of Fe signal for rat plasma sample spiked with Ferumoxytol detected with spICP-MS using a 0.1 ms dwell time(a); particle size distribution of rat plasma sample (b) spiked with IONPs (Ferumoxytol), obtained using the MassHunter software showing a indicating a median particle diameter of 52 ± 0.8 nm.

Figure 9. Time scan of Fe signal for a non-spiked rat plasma sample detected with spICP-MS using a 0.1 ms dwell time (a); particle size distribution of non-spiked rat plasma sample (b). An average median diameter of 25.8 ± 1.7 nm was detected which suggested a release of colloidal iron into the plasma from lysis of erythrocytes during possibly sample centrifugation.

From Figure 8, spICP-MS analysis of rat blood plasma spiked with Ferumoxytol showed a median particle diameter of 52 ± 0.8 nm compared with that of pristine Ferumoxytol (28±3.2 nm), indicating the detection of more larger sized NPs compared thereby suggesting the formation of large aggregates of Fe-NPs. The LOSD was 18 nm, which suggests an elevated background signal compared to the timescan of the pristine IONPs, which appears to reflect the capture of both small and big sized particles. It can be further argued that haemolysis during processing (centrifugation) releases natural Fe-containing colloids from erythrocytes into plasma; because the plasma sample was red instead of the regular straw colour of non-haemolysed plasma [51,52] (Figure 9). This is indicated by the timescan (Figure 9a) and size distribution (Figure 9b) which suggests the presence of colloidal iron in the non-spiked plasma, though ^{56}Fe signal intensity is less than that of the spiked plasma by one order of

magnitude ($x10^8$ vs $x10^7$). Comparison of the spICP-MS median diameter of 52 ± 0.8 nm (mathematical radius of 26 ± 0.2 nm) with the average particle radius of 49 nm detected with MALS for IONPs spiked into plasma may suggest the presence of a corona or around the particle core estimated at 23nm. The average equivalent circular diameter (18 nm) of the IONPS spiked into plasma determined using TEM is lower than the spICP-MS value (52 nm); a discrepancy attributed to the assumption of a spherical geometry for metallic NPs according to spICP-MS theory for the calculation of particle size. Contrarily, TEM images show the presence of non-spherical or rod-like particles thereby subjecting the spICP-MS value to bias.

Figure 10. Time scan of Fe signal for rat blood cells spiked with IONPs (Ferumoxytol) detected with spICP-MS using a 0.1 ms dwell time. (b) Particle size distribution of rat blood cell fraction spiked with Ferumoxytol, otained with the Masshunter software indicating a median particle diameter of 33 ± 2.0 nm.

In Figure 10, the cell fraction spiked with Ferumoxytol showed the detection of a median particle diameter of 33 ± 2.0 nm, with a monodisperse distribution profile similar to that of pristine IONPs. Though the particle diameter suggested a slight increase in diameter of the iron core, it does not provide conclusive evidence for aggregation of the IONP. The LOSD was11.5 nm, suggesting an increased background signal which may associated with the sample matrix. Also, while the spICP-MS distribution profile is monodisperse, the weak MALS signal for the IONPs spiked into blood cells within the iron containing fraction prevents a comparison with the spICP-MS particle diameter. The spICP-MS frequency distribution profile (Figure 10b) also shows that the particles were < 50 nm which was

similar to the size distribution of the pristine IONPs; an evidence suggesting a minimal size alteration of the IONP in the blood cell fraction. Remarkably, the mean TEM average equivalent circular particle diameter 111± 14.5 nm obtained for IONPs spiked into cell fraction shows a discrepancy with the spICP-MS particle diameter. This may indicate that the equivalent circular diameters obtained from ImageJ data analysis are incongruent with the actual shape of the particulate structures visualised in the TEM micrographs. Furthermore, TEM is a non-specific technique and endogenous natural NPs, colloids and cellular debris may be mistaken for the IONP. Another possibility is that contrary to the theoretical assumptions of spICP-MS technique of a spherical geometry to calculate particle size, the geometry of the IONPs after their spiking into the blood cell are actually not spherical as seen from TEM images, hence calculated spICP-MS particle sizes may be subject to bias. Table 1 summarises the particle sizes of the pristine IONPs and the sizes of the IONPs after spiking into rat blood plasma and cells using the different techniques applied in this study.

Table 1. Summary of IONP particle sizes obtained with the different techniques

Sample fraction	**TEM (Average particle diameter, nm)**	**MALS (Average Radius of gyration, R_g, nm)**	**spICP-MS (Median Particle diameter, nm)**
Pristine IONP	21	23	28
IONP (plasma)	18	49	52
IONP (cells)	110	-	33

Manufacturer's nominal diameter (TEM) for IONPs = 27 nm

4. Conclusion

This study has shed some light on the physico-chemical behaviour and characterisation of IONPs such as Ferumoxytol when injected into blood matrix. The characterization and applications of IONPs with various analytical techniques have been studied extensively [43,53-55]. For instance, Lohrke *et al*. [43] synthesised pristine SPIONs which they characterised using AF4-UV-MALS, DLS and TEM. However, this *in vitro* model with spiking experiments using AF4-UV-MALS-ICP-MS/MS combined with TEM and spICP-MS yet to be reported from available literature. TEM images shows that the cluster structure of the IONPs is altered in blood plasma and the IONPs become polydisperse. Despite the reported 24 h clearance rates of IONPs from reticulo-endothelial circulation (RES), there is previous experimental evidence showing that they may persist in trace amounts for an extended duration [56]. Studies by Lacava *et al*. [57] using mice have reported that injected dextran coated IONPs are cleared and stored in the liver and spleen from 1h and up to 6 months after administration. We have demonstrated that using spICP-MS analysis, the concentration of the IONPs is high enough to be detected after 24 h incubation of the IONPs and complexity of the matrix. This may have implications for potential iron overload and risk of the formation of reactive oxygen species (ROS) though the Fenton reaction [58]. However, the exact biochemical transformations of injected IONPs *in vivo* cannot be fully explained with a spiking experiment. The use of a surfactant-based mobile phase as applied in this study for AF4 separation is known to enhance NP recovery by shielding surface charge by reducing membrane adhesion and NP aggregation; however they are prone to cause an overestimation of particle sizes and micelle formation which are potential sources of measurement bias. A low intensity MALS signal for the IONPs in blood cell suggested a possible dissolution of the NP carbohydrate coating which prevented size determination of the IONPs spiked into blood cell. Thus, it was not possible to understand the precise nature of the possible size and surface modification of the IONP, which is important in the light of reported cases of hypersensitivity

and toxicity arising from the intravenous administration of IONPs and other intravenous iron products in humans [15,59].

Declaration of interest: none

ACKNOWLEDGEMENT

KN gratefully acknowledges the University of Aberdeen for an Elphinstone Ph.D. studentship and the Niger Delta Development Commission (NDDC) for a research grant (RG-13451-10). The authors also gratefully acknowledge Postnova Analytics UK especially Dr Bassem Sabagh for the loan of the AF4 system together with training, support, and advice on the technique. Microscopy was performed at the Microscopy and Histology Core facility, University of Aberdeen.

[1] S. Mura, P. Couvreur, Nanotheranostics for personalized medicine, Adv.Drug Deliv.Rev. 64 (2012) 1394-1416.

[2] S. Kunjachan, J. Ehling, G. Storm, F. Kiessling, T. Lammers, Noninvasive imaging of nanomedicines and nanotheranostics: principles, progress, and prospects, Chem.Rev. 115 (2015) 10907-10937.

[3] E. Blanco, H. Shen, M. Ferrari, Principles of nanoparticle design for overcoming biological barriers to drug delivery, Nat.Biotechnol. 33 (2015) 941.

[4] I. Khan, K. Saeed, I. Khan, Nanoparticles: Properties, applications and toxicities, Arabian Journal of Chemistry. (2017) doi://doi.org/10.1016/j.arabjc.2017.05.011.

[5] M. Mahmoudi, S. Sant, B. Wang, S. Laurent, T. Sen, Superparamagnetic iron oxide nanoparticles (SPIONs): development, surface modification and applications in chemotherapy, Adv.Drug Deliv.Rev. 63 (2011) 24-46.

[6] D.K. Kim, M. Mikhaylova, Y. Zhang, M. Muhammed, Protective coating of superparamagnetic iron oxide nanoparticles, Chemistry of Materials. 15 (2003) 1617-1627.

[7] A.K. Gupta, M. Gupta, Synthesis and surface engineering of iron oxide nanoparticles for biomedical applications, Biomaterials. 26 (2004) 3995-4221.

[8] D. Askri, S. Ouni, S. Galai, B. Chovelon, J. Arnaud, S.G. Lehmann, M. Sakly, M. Sève, S. Amara, Sub-acute intravenous exposure to Fe 2 O 3 nanoparticles does not alter cognitive performances and catecholamine levels, but slightly disrupts plasma iron level and brain iron content in rats, Journal of Trace Elements in Medicine and Biology. (2018).

[9] C.G. Varallyay, G.B. Toth, R. Fu, J.P. Netto, J. Firkins, P. Ambady, E.A. Neuwelt, What Does the Boxed Warning Tell Us? Safe Practice of Using Ferumoxytol as an MRI Contrast Agent, AJNR Am.J.Neuroradiol. 38 (2017) 1297-1302.

[10] E.A. Neuwelt, B.E. Hamilton, C.G. Varallyay, W.R. Rooney, R.D. Edelman, P.M. Jacobs, S.G. Watnick, Ultrasmall superparamagnetic iron oxides (USPIOs): a future alternative magnetic resonance (MR) contrast agent for patients at risk for nephrogenic systemic fibrosis (NSF)?, Kidney Int. 75 (2009) 465-474.

[11] I.C. Macdougall, P. Geisser, Use of Intravenous Iron Supplementation in Chronic Kidney Disease An Update., Iranian journal of kidney diseases. 7 (2013).

[12] S.S. Vasanawala, K. Nguyen, M.D. Hope, M.D. Bridges, T.A. Hope, S.B. Reeder, M.R. Bashir, Safety and technique of ferumoxytol administration for MRI, Magnetic resonance in medicine. 75 (2016) 2107-2111.

[13] T. Johnson-Wimbley, D.Y. Graham, Diagnosis and management of iron deficiency anemia in the 21st century, Therap Adv Gastroenterol. 4 177-184.

[14] M. Auerbach, Ferumoxytol as a new, safer, easier-to-administer intravenous iron: yes or no?, American Journal of Kidney Diseases. 52 (2008) 826-829.

[15] S. Santosh, P. Podaralla, B. Miller, Anaphylaxis with elevated serum tryptase after administration of intravenous ferumoxytol, NDT plus. 3 (2010) 341-342.

[16] N.F. Olivieri, G.M. Brittenham, Iron-chelating therapy and the treatment of thalassemia, Blood. 89 (1997) 739-761.

[17] S.J. Dixon, B.R. Stockwell, The role of iron and reactive oxygen species in cell death, Nature chemical biology. 10 (2014) 9.

[18] M.R. Mohammadi, A.V. Malkovskiy, P. Jothimuthu, K. Kim, M. Parekh, M. Inayathullah, Y. Zhuge, J. Rajadas, PEG/Dextran Double Layer Influences Fe Ion Release and Colloidal Stability of Iron Oxide Nanoparticles, Scientific reports. 8 (2018) 4286.

[19] US Food and Drug Administration, FDA Drug Safety Communication: FDA strengthens warnings and changes prescribing instructions to decrease the risk of serious allergic reactions with anemia drug Feraheme (ferumoxytol), FDA web-site. (2015).

[20] C. Huang, C. Tsai, H. Sheu, K. Chuang, C. Su, U. Jeng, F. Cheng, C. Su, H. Lei, C. Yeh, Enhancing transversal relaxation for magnetite nanoparticles in MR imaging using Gd3 - chelated mesoporous silica shells, ACS nano. 5 (2011) 3905-3916.

[21] L.H. Bryant Jr, S.J. Kim, M. Hobson, B. Milo, Z.I. Kovacs, N. Jikaria, B.K. Lewis, M.A. Aronova, A.A. Sousa, G. Zhang, Physicochemical characterization of ferumoxytol, heparin and protamine nanocomplexes for improved magnetic labeling of stem cells, Nanomedicine: Nanotechnology, Biology and Medicine. 13 (2017) 503-513.

[22] Y. Wu, P. Petrochenko, L. Chen, S.Y. Wong, M. Absar, S. Choi, J. Zheng, Core size determination and structural characterization of intravenous iron complexes by cryogenic transmission electron microscopy, Int.J.Pharm. 505 (2016) 167-174.

[23] F.v.d. Kammer, S. Legros, T. Hofmann, E.H. Larsen, K. Loeschner, Separation and characterization of nanoparticles in complex food and environmental samples by field-flow fractionation, TrAC Trends in Analytical Chemistry. 30 425-436. doi://doi.org/10.1016/j.trac.2010.11.012.

[24] W. Fraunhofer, G. Winter, The use of asymmetrical flow field-flow fractionation in pharmaceutics and biopharmaceutics, European Journal of Pharmaceutics and Biopharmaceutics. 58 (2004) 369-383.

[25] C. Contado, Field flow fractionation techniques to explore the "nano-world", Analytical and bioanalytical chemistry. 409 (2017) 2501-2518.

[26] C. Fuentes, J. Castillo, J. Vila, L. Nilsson, Application of asymmetric flow field-flow fractionation (AF4) and multiangle light scattering (MALS) for the evaluation of changes in the product molar mass during PVP-b-PAMPS synthesis, Analytical and bioanalytical chemistry. 410 (2018) 3757-3767.

[27] R. Stepto, T. Chang, P. Kratochvíl, M. Hess, K. Horie, T. Sato, J. Vohlídal, Definitions of terms relating to individual macromolecules, macromolecular assemblies, polymer solutions, and amorphous bulk polymers (IUPAC Recommendations 2014), Pure and Applied Chemistry. 87 (2015) 71-120.

[28] B. Meermann, K. Wichmann, F. Lauer, F. Vanhaecke, T.A. Ternes, Application of stable isotopes and AF4/ICP-SFMS for simultaneous tracing and quantification of iron oxide nanoparticles in a sediment–slurry matrix, J.Anal.At.Spectrom. 31 (2016) 890-901.

[29] B. Meermann, A. Fabricius, L. Duester, F. Vanhaecke, T. Ternes, Fraction-related quantification of silver nanoparticles via on-line species-unspecific post-channel isotope dilution in combination with asymmetric flow-field-flow fractionation (AF4)/sector field ICP-mass spectrometry (ICP-SF-MS), J.Anal.At.Spectrom. 29 (2014) 287-296.

[30] H. El Hadri, S.M. Louie, V.A. Hackley, Assessing the interactions of metal nanoparticles in soil and sediment matrices–a quantitative analytical multi-technique approach, Environmental Science: Nano. 5 (2018) 203-214.

[31] B. Meermann, V. Nischwitz, ICP-MS for the Analysis at the Nanoscale-A tutorial Review, J.Anal.At.Spectrom. (2018).

[32] E.P. Gray, J.G. Coleman, A.J. Bednar, A.J. Kennedy, J.F. Ranville, C.P. Higgins, Extraction and analysis of silver and gold nanoparticles from biological tissues using single

particle inductively coupled plasma mass spectrometry, Environ.Sci.Technol. 47 (2013) 14315-14323.

[33] H.E. Pace, N.J. Rogers, C. Jarolimek, V.A. Coleman, E.P. Gray, C.P. Higgins, J.F. Ranville, Single particle inductively coupled plasma-mass spectrometry: a performance evaluation and method comparison in the determination of nanoparticle size, Environ.Sci.Technol. 46 (2012) 12272-12280.

[34] A.C. Makan, M.J. Spallek, M. du Toit, T. Klein, H. Pasch, Advanced analysis of polymer emulsions: Particle size and particle size distribution by field-flow fractionation and dynamic light scattering, Journal of Chromatography A. 1442 (2016) 94-106. doi://doi.org/10.1016/j.chroma.2016.03.013.

[35] A.K. Gupta, A.S.G. Curtis, Lactoferrin and ceruloplasmin derivatized superparamagnetic iron oxide nanoparticles for targeting cell surface receptors, Biomaterials. 25 3029-3040. doi://doi.org/10.1016/j.biomaterials.2003.09.095.

[36] B. Diaz, C. Sánchez- Espinel, M. Arruebo, J. Faro, E. de Miguel, S. Magadán, C. Yagüe, R. Fernández- Pacheco, M.R. Ibarra, J. Santamaria, Assessing methods for blood cell cytotoxic responses to inorganic nanoparticles and nanoparticle aggregates, Small. 4 (2008) 2025-2034.

[37] P.R. Chang, J. Yu, X. Ma, D.P. Anderson, Polysaccharides as stabilizers for the synthesis of magnetic nanoparticles, Carbohydrate Polymers. 83 (2011) 640-644. doi://doi.org/10.1016/j.carbpol.2010.08.027.

[38] H. Dou, E.C. Jung, S. Lee, Factors affecting measurement of channel thickness in asymmetrical flow field-flow fractionation, Journal of Chromatography A. 1393 (2015) 115-121.

[39] S. Du, K. Kendall, P. Toloueinia, Y. Mehrabadi, G. Gupta, J. Newton, Aggregation and adhesion of gold nanoparticles in phosphate buffered saline, Journal of nanoparticle research. 14 (2012) 758.

[40] K. Afshinnia, M. Baalousha, Effect of phosphate buffer on aggregation kinetics of citrate-coated silver nanoparticles induced by monovalent and divalent electrolytes, Science of The Total Environment. 581-582 (2017) 268-276. doi://doi.org/10.1016/j.scitotenv.2016.12.117.

[41] M.E. Schimpf, K. Caldwell, J.C. Giddings, Field-Flow Fractionation Handbook.John Wiley & Sons, 2000.

[42] A.F. Thünemann, S. Rolf, P. Knappe, S. Weidner, In situ analysis of a bimodal size distribution of superparamagnetic nanoparticles, Anal.Chem. 81 (2008) 296-301.

[43] J. Lohrke, A. Briel, K. Mäder, Characterization of superparamagnetic iron oxide nanoparticles by asymmetrical flow-field-flow-fractionation, Nanomedicine. 3 (2008) 437-452.

[44] J. Gigault, J.M. Pettibone, C. Schmitt, V.A. Hackley, Rational strategy for characterization of nanoscale particles by asymmetric-flow field flow fractionation: A tutorial, Analytica Chimica Acta. 809 (2014) 9-24. doi://doi.org/10.1016/j.aca.2013.11.021.

[45] Z. Hu, H. Zhang, Y. Zhang, R. Wu, H. Zou, Nanoparticle size matters in the formation of plasma protein coronas on Fe3O4 nanoparticles, Colloids and Surfaces B: Biointerfaces. 121 (2014) 354-361. doi://doi.org/10.1016/j.colsurfb.2014.06.016.

[46] Y. Wang, Y.W. Ng, Y. Chen, B. Shuter, J. Yi, J. Ding, S. Wang, S. Feng, Formulation of superparamagnetic iron oxides by nanoparticles of biodegradable polymers for magnetic resonance imaging, Advanced Functional Materials. 18 (2008) 308-318.

[47] F. Laborda, E. Bolea, J. Jiménez-Lamana, No title, Single particle inductively coupled plasma mass spectrometry: a powerful tool for nanoanalysis. (2013).

[48] H.E. Pace, N.J. Rogers, C. Jarolimek, V.A. Coleman, C.P. Higgins, J.F. Ranville, Determining transport efficiency for the purpose of counting and sizing nanoparticles via single particle inductively coupled plasma mass spectrometry, Anal.Chem. 83 (2011) 9361-9369.

[49] C. Degueldre, P. Favarger, Colloid analysis by single particle inductively coupled plasma-mass spectroscopy: a feasibility study, Colloids Surf.Physicochem.Eng.Aspects. 217 (2003) 137-142.

[50] S. Lee, X. Bi, R.B. Reed, J.F. Ranville, P. Herckes, P. and Westerhoff, Nanoparticle Size Detection Limits by Single Particle ICP-MS for 40
Elements, Environmental Science and Technology. 48 (2014) 10291-10300.

[51] S.O. Sowemimo-Coker, Red blood cell hemolysis during processing, Transfusion Medicine Reviews. 16 46-60. doi://doi.org/10.1053/tmrv.2002.29404.

[52] M. Daves, V. Roccaforte, M. Giacomi, M. Riva, M. Leitner, S. Platzgummer, G. Goetsch, G. Lippi, Effect of delayed centrifugation of whole blood on serum samples stability, La Rivista Italiana della Medicina di Laboratorio-Italian Journal of Laboratory Medicine. 13 (2017) 41-44.

[53] H. Wei, O.T. Bruns, M.G. Kaul, E.C. Hansen, M. Barch, A. Wisniowska, O. Chen, Y. Chen, N. Li, S. Okada, J.M. Cordero, M. Heine, C.T. Farrar, D.M. Montana, G. Adam, H. Ittrich, A. Jasanoff, P. Nielsen, M.G. Bawendi, Exceedingly small iron oxide nanoparticles as positive MRI contrast agents, Proc.Natl.Acad.Sci.U.S.A. 114 (2017) 2325-2330.

[54] Y. Huang, B. Zhang, S. Xie, B. Yang, Q. Xu, J. Tan, Superparamagnetic iron oxide nanoparticles modified with Tween 80 pass through the intact blood–brain barrier in rats under magnetic field, ACS applied materials & interfaces. 8 (2016) 11336-11341.

[55] M.P. Sutunkovaa, B.A. Katsnelsona, L.I. Privalovaa, V.B. Gurvicha, L.K. Konyshevaa, V.Y. Shurb, E.V. Shishkinab, I.A. Minigalievaa, S.N. Solovjevaa, S.V. Grebenkinaa, I.V. Zubarevb, On the contribution of the phagocytosis and the solubilization to the iron oxide nanoparticles retention in and elimination from lungs under long-term inhalation exposure., Toxicology. 363 (2016) 19-28.

[56] M.R. Bashir, L. Bhatti, D. Marin, R.C. Nelson, Emerging applications for ferumoxytol as a contrast agent in MRI, Journal of Magnetic Resonance Imaging. 41 (2015) 884-898.

[57] L.M. Lacava, V.A.P. Garcia, S. Kückelhaus, R.B. Azevedo, N. Sadeghiani, N. Buske, P.C. Morais, Z.G.M. Lacava, Long-term retention of dextran-coated magnetite nanoparticles in the liver and spleen, Journal of Magnetism and Magnetic Materials. 272-276 2434-2435. doi://doi.org/10.1016/j.jmmm.2003.12.852.

[58] N. Singh, G.J. Jenkins, R. Asadi, S.H. Doak, Potential toxicity of superparamagnetic iron oxide nanoparticles (SPION), Nano reviews. 1 (2010) 5358.

[59] M. Zhu, B. Wang, Y. Wang, L. Yuan, H. Wang, M. Wang, H. Ouyang, Z. Chai, W. Feng, Y. Zhao, Endothelial dysfunction and inflammation induced by iron oxide nanoparticle exposure: Risk factors for early atherosclerosis, Toxicol.Lett. 203 (2011) 162-171.

Highlights

- A monodisperse distribution was obtained for pristine iron oxide NPs.
- TEM showed that IONPs were polydisperse when spiked into blood plasma.
- A weak MALS signal for IONPs spiked in blood cell suggested NP loss.
- IONPs sizes in plasma were affected by colloidal Fe release by cell lysis.
- spICP-MS indicated that NP size changes was due to sample matrix effects.

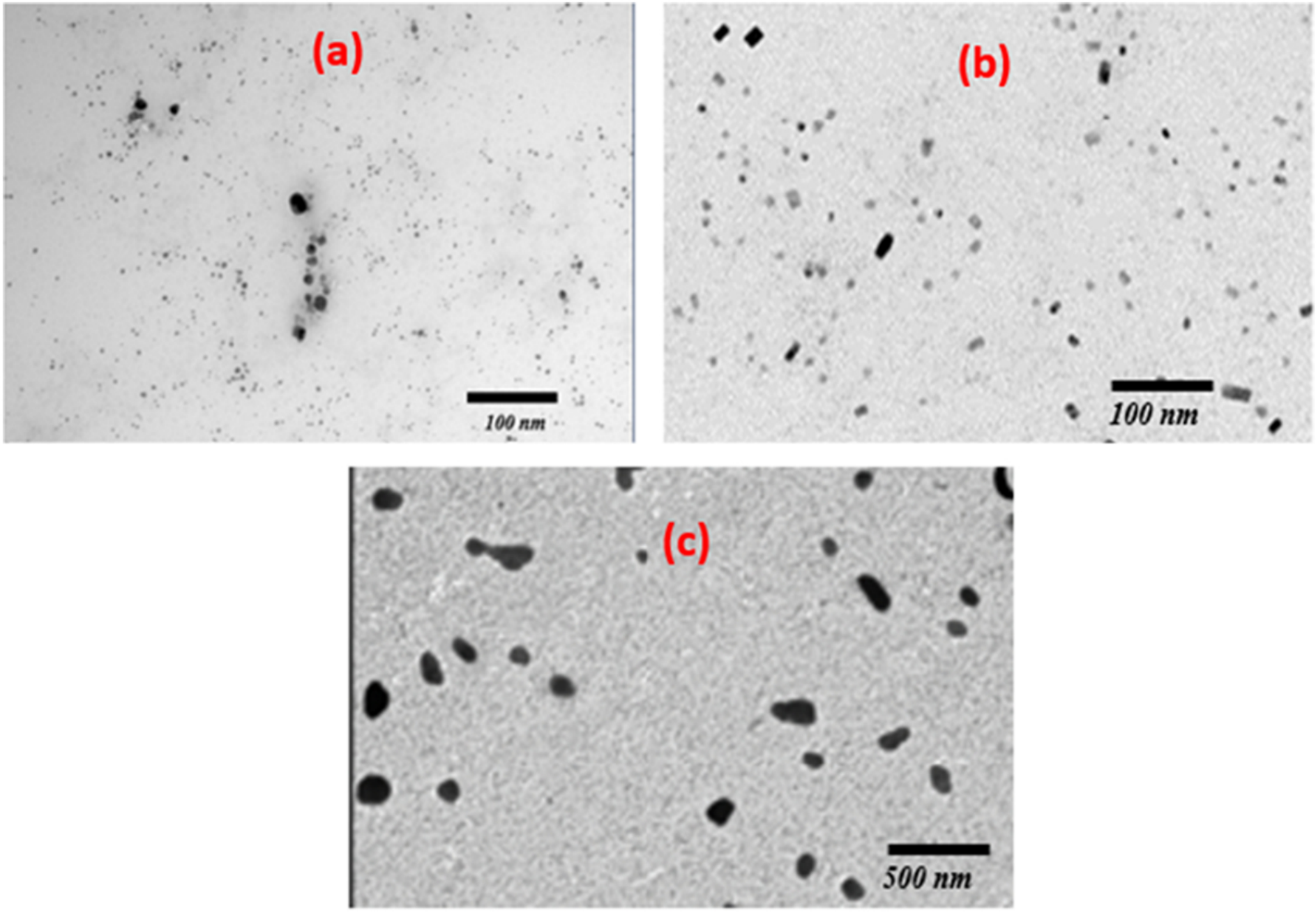

Figure 1

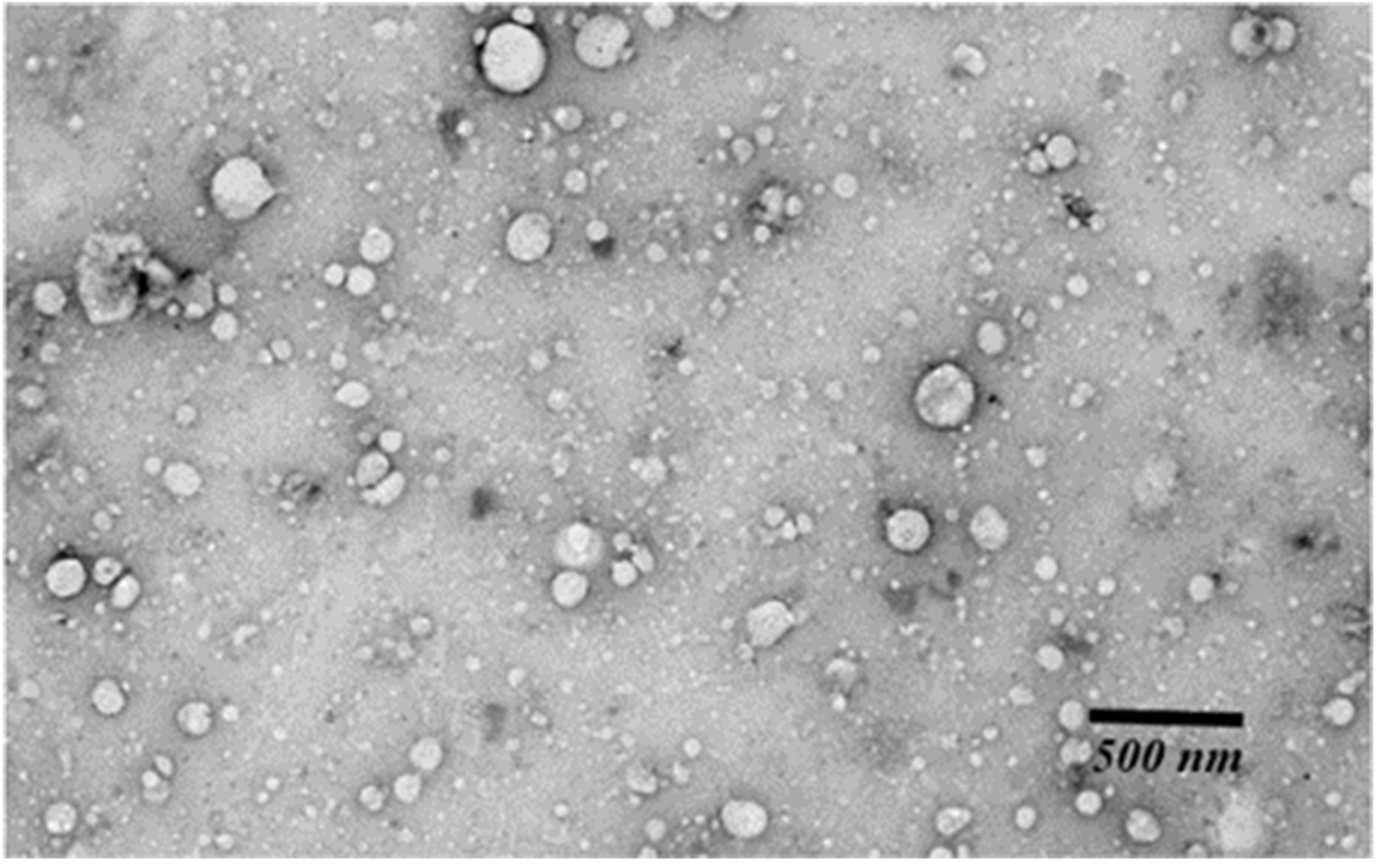

Figure 2

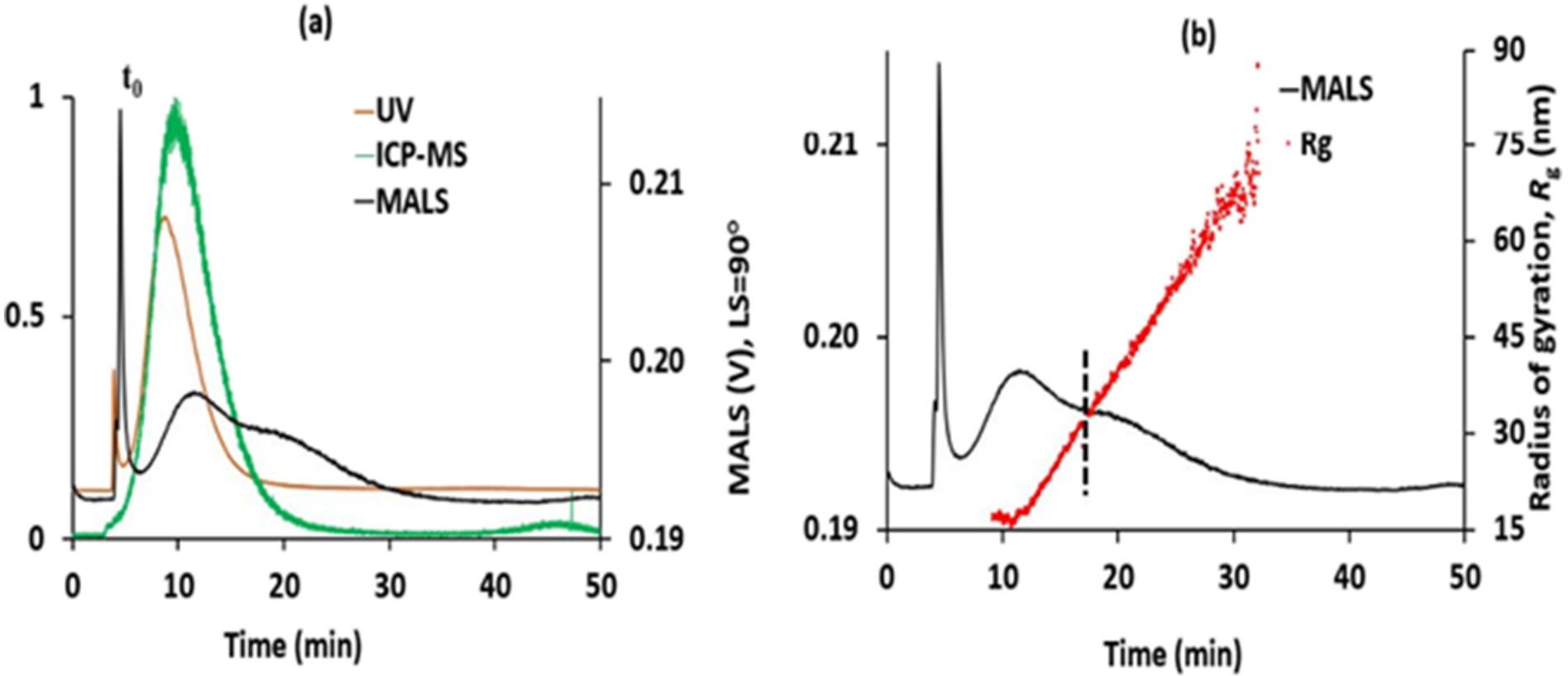
(a)
t0
UV
ICP-MS
MALS
1
0.5
0
0.21
0.20
0.19
0
10
20
30
40
50
Time (min)
(b)
MALS
Rg
MALS (V), LS=90°
Radius of gyration, Rg (nm)
0.21
0.20
0.19
90
75
60
45
30
15
0
10
20
30
40
50
Time (min)

Figure 3

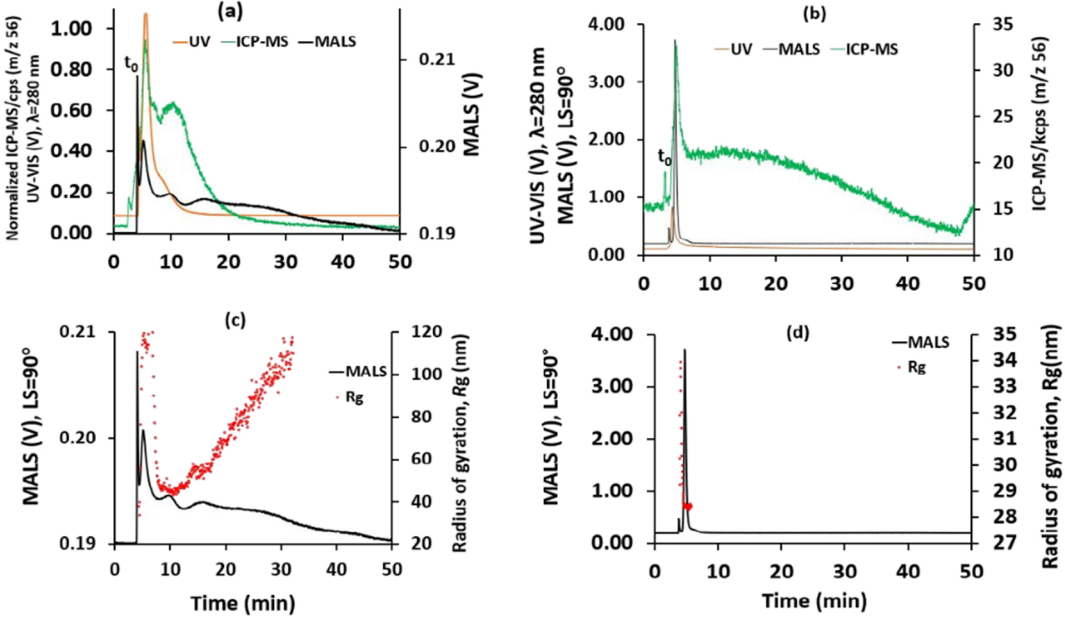
(a)
UV
ICP-MS
MALS
t_0
Normalized ICP-MS/cps (m/z 56)
UV-VIS (V), λ=280 nm
MALS (V)
(b)
UV
MALS
ICP-MS
t_0
UV-VIS (V), λ=280 nm
MALS (V), LS=90°
ICP-MS/kcps (m/z 56)
(c)
MALS
Rg
MALS (V), LS=90°
Radius of gyration, Rg (nm)
Time (min)
(d)
MALS
Rg
MALS (V), LS=90°
Radius of gyration, Rg(nm)
Time (min)

Figure 4

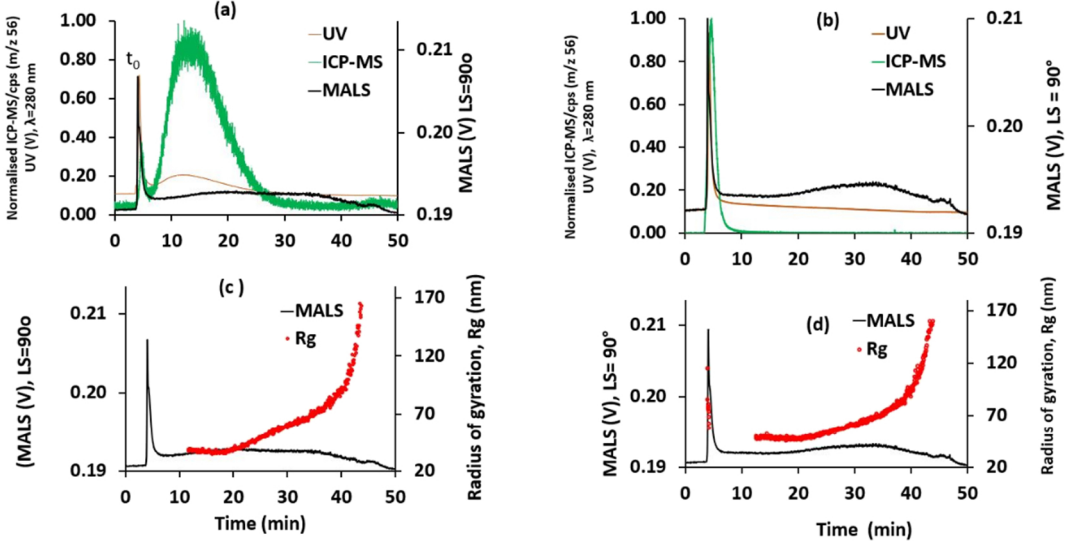
(a)
UV
ICP-MS
MALS
t_0
Normalised ICP-MS/cps (m/z 56)
UV (V), λ=280 nm
MALS (V) LS=90o
(b)
UV
ICP-MS
MALS
Normalised ICP-MS/cps (m/z 56)
UV (V), λ=280 nm
MALS (V), LS = 90°
(c)
MALS
Rg
(MALS (V), LS=90o
Radius of gyration, Rg (nm)
Time (min)
(d)
MALS
Rg
MALS (V), LS= 90°
Radius of gyration, Rg (nm)
Time (min)

Figure 5

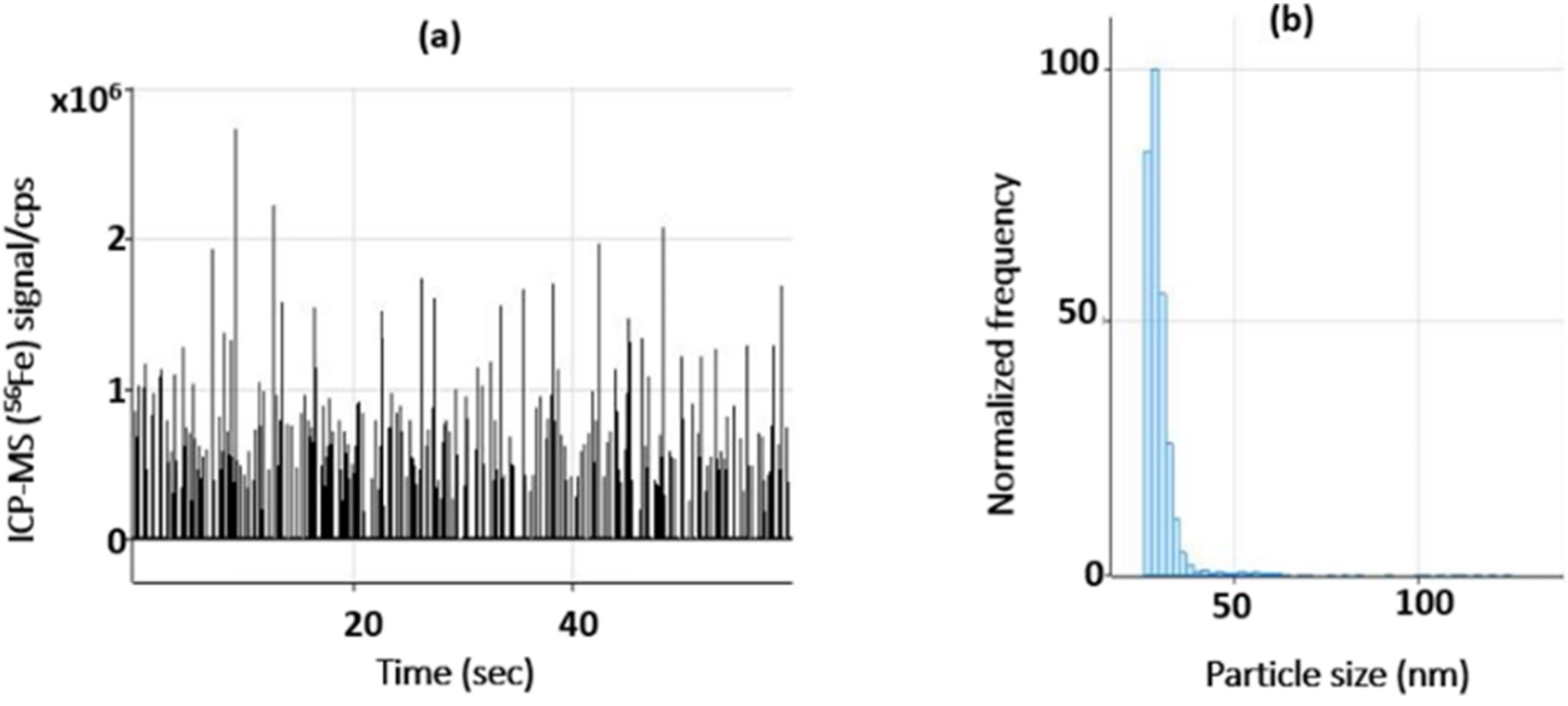
(a)
x10^6
2
1
0
ICP-MS (56Fe) signal/cps
20
40
Time (sec)
(b)
100
50
0
Normalized frequency
50
100
Particle size (nm)

Figure 6

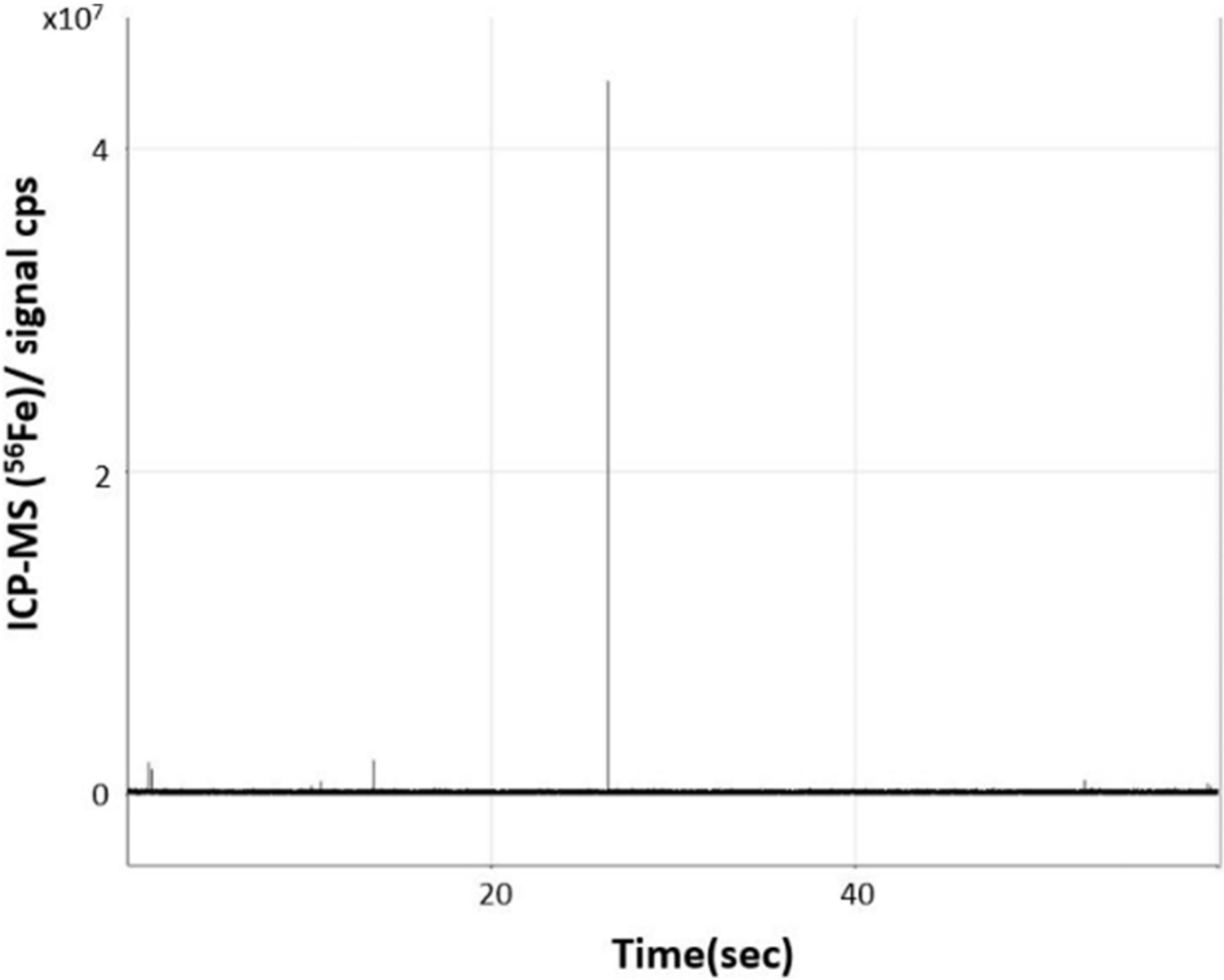

Figure 7

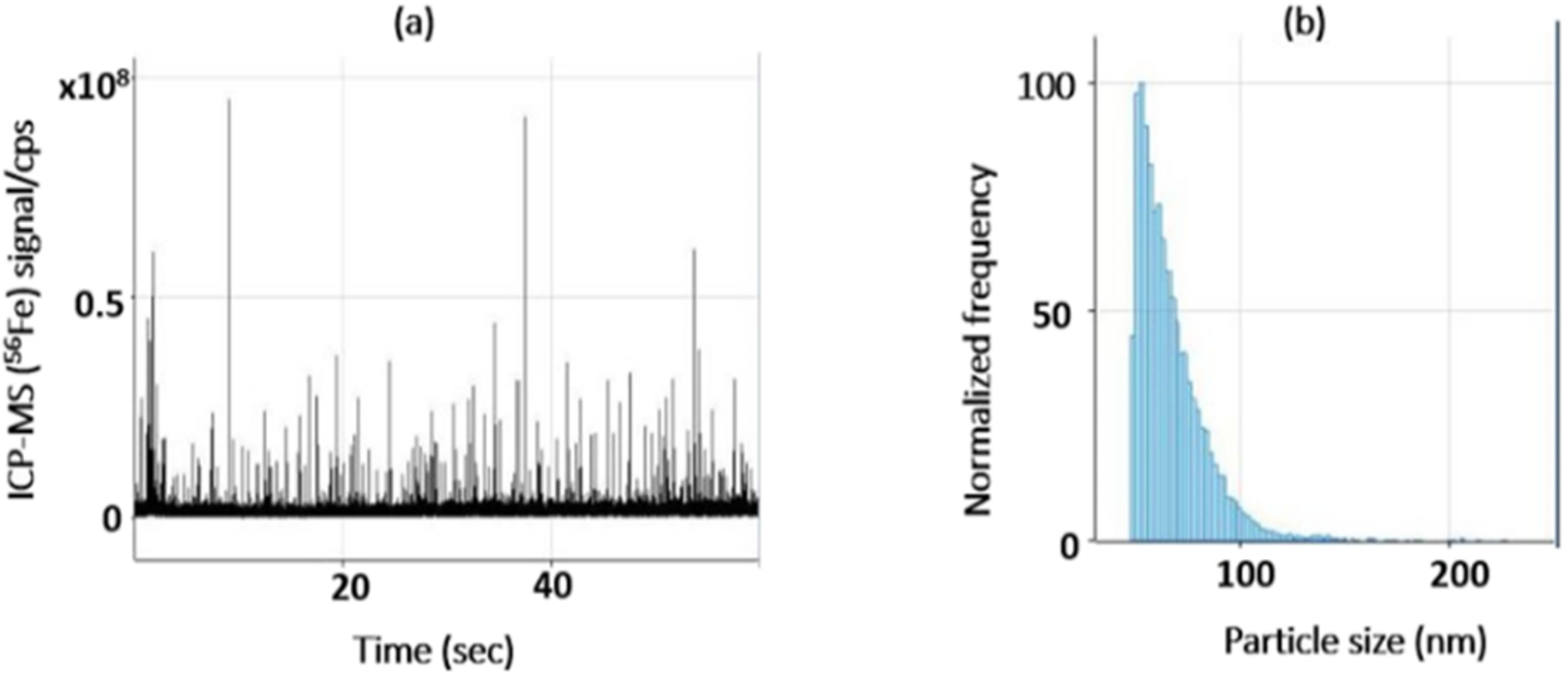
(a)
x10^8
0.5
0
ICP-MS (56Fe) signal/cps
20
40
Time (sec)
(b)
100
50
0
Normalized frequency
100
200
Particle size (nm)

Figure 8

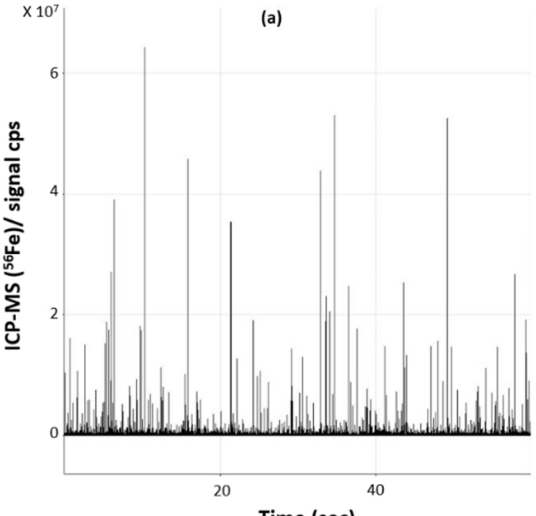
X 10^7
(a)
ICP-MS (56Fe)/ signal cps
6
4
2
0
20
40
Time (sec)

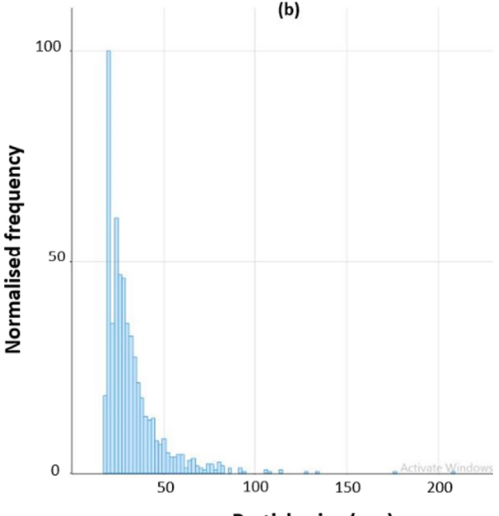
(b)
Normalised frequency
100
50
0
50
100
150
200
Particle size (nm)
Activate Windows

Figure 9

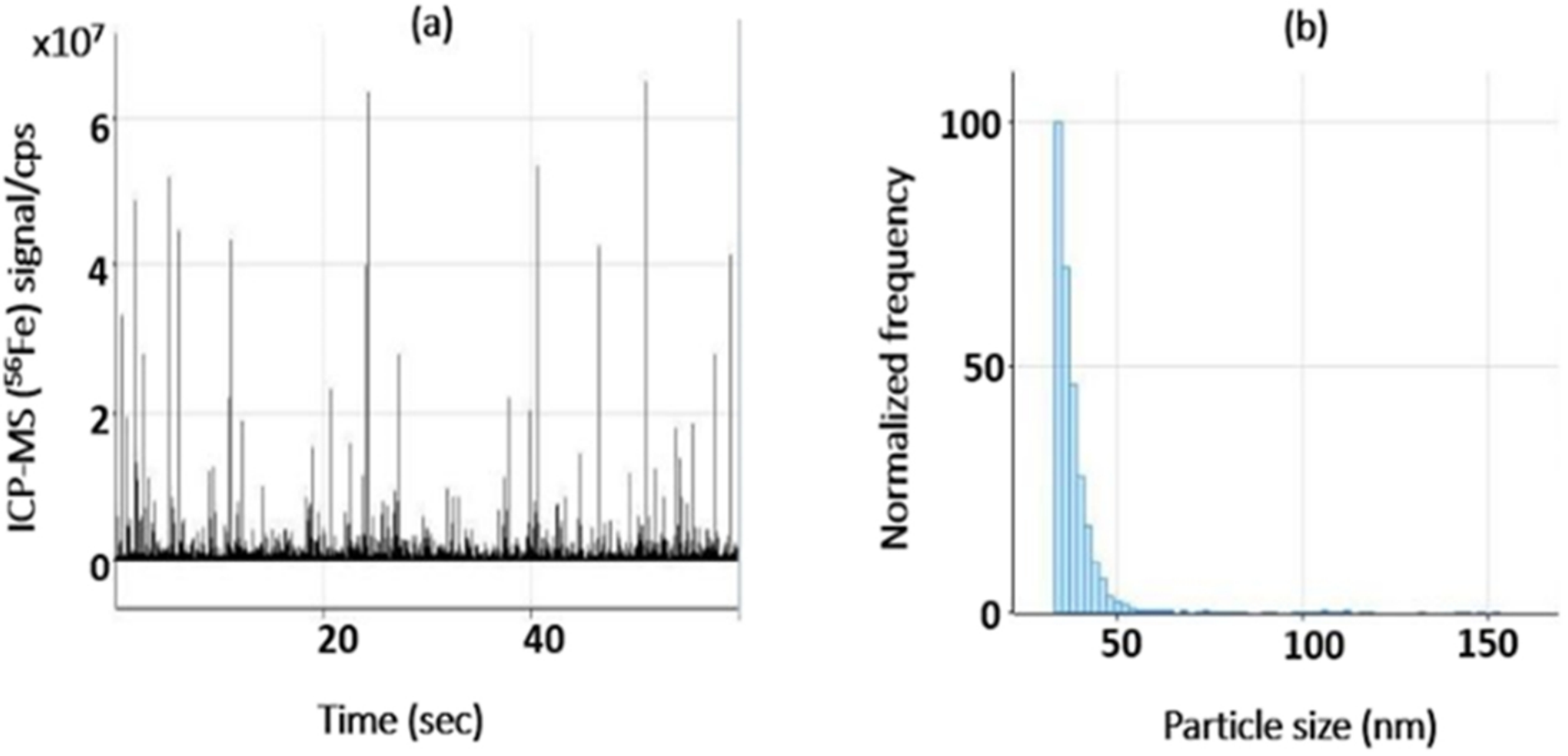
(a)
x10⁷
6
4
2
0
ICP-MS (⁵⁶Fe) signal/cps
20
40
Time (sec)
(b)
100
50
0
Normalized frequency
50
100
150
Particle size (nm)

Figure 10